Transactions of the Materials Research Society of Japan 29[4] 1585-1590 (2004)

Interlayer Exchange Coupling across Epitaxial Tunnel Barriers Consisting of Si Layers or Si-Ge Layered Structures

D.E. Bürgler, R.R. Gareev, L.L. Pohlmann, H. Braak, M. Buchmeier, R. Schreiber, and P.A. Grünberg
Institut für Festkörperforschung, Forschungszentrum Jülich GmbH, D-52425 Jülich, Germany
Fax: 49-2461-614444, e-mail: D.Buergler@fz-juelich.de

We review Kerr effect and Brillouin light scattering data revealing antiferromagnetic interlayer exchange coupling (AFC) of Fe layers across epitaxial spacers of either Si or Ge layers combined with Si (boundary-) layers. In both cases AFC is observed and decays with spacer thickness on a length scale of 2-3 Å. For Fe/Si/Fe structures, we use transport measurements of lithographically structured junctions in current-perpendicular-plane geometry to characterize the interlayers by checking the validity of the three "Rowell criteria" for tunneling: (i) exponential increase of resistance R with thickness of the barrier, (ii) parabolic dI/dV-V curves, and (iii) slight decrease of R with increasing temperature. Fe/Si/Fe samples with 14-17 Å-thick interlayers show AFC of the order of 0.5 mJ/m^2 and fulfill all three Rowell criteria proving that AFC can occur across tunneling barriers, *i.e.* across a non-conducting spacer. Samples with Ge-containing interlayers reveal AFC of the order of 1 mJ/m^2 when we use Si boundary layers to prevent direct contact between Fe and Ge or when the spacer consists of a Si-Ge-multilayer. The latter structures are of better growth quality giving rise to almost pure bilinear coupling. The interlayer coupling behavior across nominally pure Si and Ge-containing interlayers is compared and discussed.

Key words: Interlayer exchange coupling, tunneling barrier, semiconducting interlayer, Rowell criteria

1. INTRODUCTION

Recent observations of antiferromagnetic interlayer exchange coupling (AFC) across non-conducting epitaxial spacers of nominally pure Si [1] and of MgO [2] focuses particular interest on this new class of highly resistive structures exhibiting non-oscillatory AFC.

Previously, we have found that insulating-type, highly resistive Si spacers can be prepared by a certain deposition procedure [1,3,4]. Corresponding Fe/Si/Fe structures reveal very strong AFC with a total coupling strength in excess of 5 mJ/m^2 [1], which could be further increased to 8 mJ/m^2 by inserting thin epitaxial and metallic FeSi boundary layers at interfaces [4]. For combined semiconducting/metallic epitaxial spacers (*i.e.* nominally pure Si/$Fe_{0.5}Si_{0.5}$), the main impact to AFC originates from the semiconducting part of the spacer [5]. Hence, the strong and exponentially decaying AFC arises from Si-rich spacers, in qualitative agreement with the quantum interference model of exchange coupling across non-conducting spacers [6]. However, the behavior of the coupling indicated that nominally pure Si spacers are effectively inhomogeneous. For a nominal spacer thickness t less than several monolayers, the interlayer coupling becomes ferromagnetic (FM) most likely due to conducting pin-holes formed by interdiffusion at the interfaces [1,4]. For thicker spacers, the effect of pin-holes and FM coupling are expected to be suppressed.

Transport measurements with the current flowing perpendicular to the samples plane (CPP) can yield additional and clear information whether a Si-rich spacer is metallic or insulating. A further question is whether the transport in highly resistive spacers is due to elastic tunneling, or whether it arises from an additional channel of conductivity across submicron-sized pin-holes, as it was pointed out in Refs. [7,8]. In order to address these questions we examine for epitaxial Fe/Si/Fe structures the validity of the necessary and sufficient Rowell criteria for direct elastic tunneling [8], *i.e.* (i) strong and exponential increase of the resistance R with t, (ii) parabolic dependence of conductivity *versus* bias voltage, and —most decisive— (iii) small and negative temperature coefficient of the zero-bias resistance [9].

Additionally we address the question whether the observed strong AFC across Si is a specific property of Si or maybe of the combination of Fe and Si. In order to investigate the existence and the properties of AFC across another semiconductor than Si, we present experiments dealing with Fe layers coupled across epitaxial Ge-containing spacers [10]. As it was reported previously [11], epitaxial Fe/Ge/Fe structures reveal no evidence of AFC. Therefore, we use AFC-mediating, epitaxial Si boundary layers (BL) at the interfaces towards the Fe layers to avoid direct contact of Ge with Fe and, thus, the possible formation of magnetic Fe-Ge compounds that prevent AFC [11]. The lattice mismatch of about 4% between Ge (a_{Ge}=5.66 Å) and Si (a_{Si}=5.43 Å) is known to give rise to the Stransky-Krastanov (SK) growth mode: several monolayers of strained Ge grow

epitaxially on Si, and Ge hillocks form for larger Ge thickness [12]. In order to avoid SK growth we also try to stabilize the strain in the spacer by piling up thin layers of Ge and Si to form Si-Ge-multilayer spacers.

2. EXPERIMENTAL PROCEDURES

2.1 Sample preparation

We grow our Fe/spacer/Fe(001) structures in a molecular-beam epitaxy system using a 150 nm-thick Ag(001) buffer system on GaAs(001) [1,3]. The layers forming the spacers are deposited at low deposition rates (<0.1 Å/s) and at room temperature (RT). For the samples with Ge-containing interlayers we distinguish three types of spacers: (i) Ge-wedges, (ii) Ge-wedges embedded between two 4 Å-thick Si BL at both the bottom and top interfaces towards the Fe layers, and (iii) Si-Ge-multilayers consisting of N alternating 2 Å-thick Si and Ge sublayers. The nominal thickness of the wedges ranges from 8 to 20 Å for Si and from 0 to 15 Å for Ge. The total thickness of the Si BL of 8 Å is chosen to obtain highly resistive spacers, which reveal strong and insulating-type AFC [1].

2.2 Magnetic and structural characterization

Magnetic properties are measured by magneto-optical Kerr effect (MOKE) in Voigt geometry and/or Brillouin light scattering from spin waves (BLS). Bilinear (J_1) and biquadratic (J_2) coupling constants are determined by fitting the field dependence of MOKE and BLS data using the usual areal energy density expression

$$E_{ex} = -J_1 \cos(\Theta) - J_2 \cos^2(\Theta) \qquad (1)$$

to phenomenologically describe interlayer exchange coupling, where Θ is the angle between the two Fe film magnetizations. The external magnetic field (H<800 mT) is applied along an easy-axis of Fe(001). For some samples types with very strong AFC, we prepared structures with constant spacer thickness and checked the antiparallel alignment by SQUID magnetometry, where we can apply higher magnetic fields and saturate the samples. Further details concerning the preparation of the structures, their characterization, and the fitting procedures are described in Refs. [1,3,13].

The in-plane crystalline structure of all layers is characterized by means of low-energy electron diffraction (LEED). An example for a sample with a Ge-wedge embedded in two Si BL is given in Fig. 1.

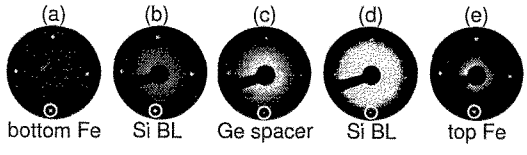

Fig. 1. LEED patterns of a Fe/BL/Ge/BL/Fe structure taken at 55 eV: (a) 50 Å bottom Fe layer, (b) 4 Å Si bottom BL, (c) 5 Å Ge spacer, (d) 4 Å Si top BL, and (e) 30 Å top Fe layer. Si BL, Ge spacer, and top Fe layer are grown at RT. Circles mark the position of the (01) spot of bcc-Fe(001) corresponding to an in-plane lattice constant of 2.9 Å (from [10]).

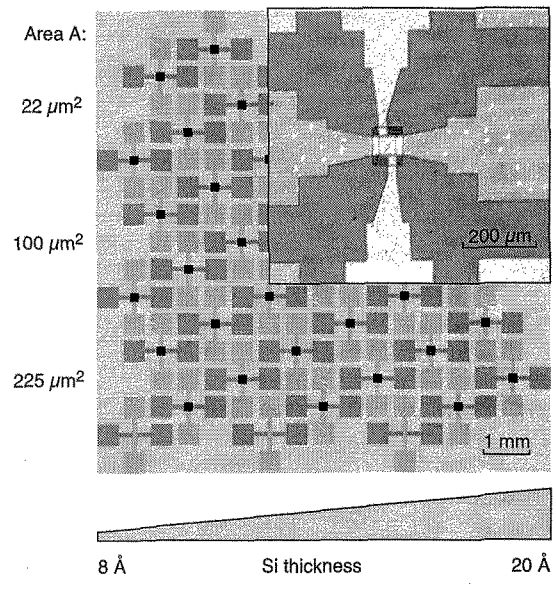

Fig. 2. Layout of the sample for CPP transport measurements after patterning. The wedge-type Si spacer layer results in junctions with different spacer thicknesses. The inset shows a photograph of a typical patterned junction (after [9]).

2.3 Lithography and transport measurements

The CPP transport measurements of the Fe/Si/Fe structures are performed after patterning 10x10 mm²-sized, wedge-type samples using photolithography, ion-beam etching, and the lift-off technique. The layout of the patterned sample is shown in Fig. 2. In this way we obtain CPP junctions with different Si spacer thicknesses t and variable junction areas A, which all are deposited under the same growth conditions. We use crossed contacts, where a 300 nm-thick Cu layer forms the upper electrode. The patterned 150 nm-thick silver buffer layer serves as a bottom electrode. The sheet resistances of both electrodes are about 0.1 Ω and thus significantly

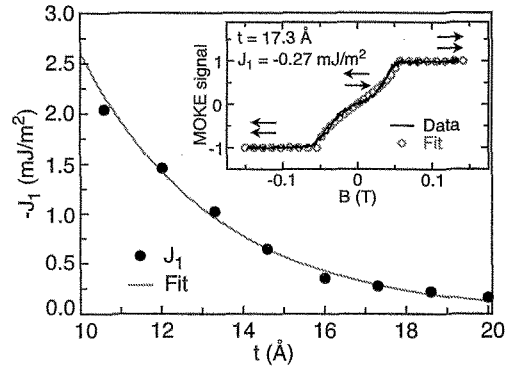

Fig. 3. Bilinear coupling constant J_1 of a Fe(50 Å)/Si(t)/Fe(50 Å) structure measured at RT *versus* spacer thickness t. The fitted curve yields a decay length of 3.3 Å. Inset: Experimental and fitted longitudinal MOKE hysteresis curves for t=17.3 Å clearly show antiparallel alignment due to AFC and yield J_1=-0.27 mJ/m² at RT (from [9]).

smaller than the resistance of the tunneling junctions in CPP geometry (5-300 Ω), such that current distribution effects are diminished [14]. Insulation of the electrodes is achieved by deposition of a 250 nm-thick Si-oxide layer. Finally, we define junctions of rectangular shape ranging in area A from 22 to more than 200 μm^2. A photograph of a typical junction is shown in the inset of Fig. 2. After patterning, voltage and current leads suitable for four-point transport measurements are connected by ultrasonic bonding to measure the *I-V* characteristics of the junctions.

3. RESULTS

3.1 AFC of Fe/Si-wedge/Fe

The thickness dependence of the bilinear coupling strength J_1 of a Fe(50 Å)/Si(8-20 Å)/Fe(50 Å) structure measured at RT before lithography is shown in Fig. 3. $|J_1|$ decays exponentially with t with a decay length of about 3 Å. For $t \approx 20$ Å the coupling strength decreases to $|J_1| \approx 0.1$ mJ/m^2. The zero-field antiparallel alignment is observed in the whole range of temperatures (4-300 K) and for all spacer thicknesses (see inset of Fig. 3).

3.2. Transport measurements of Fe/Si/Fe

First Rowell criterion: In Fig. 4 we show the resistance times area product *RA versus t* on a semi-logarithmic scale. The value of *RA* increases at RT strongly with *t* by more than 4 orders of magnitude, while *t* only approximately doubles. The characteristic length t_0 of the order of 1 Å (dashed line in Fig. 4) is significantly shorter compared to corresponding characteristic lengths for structures with amorphous Si spacers [15]. Note, that the AFC across epitaxial, Si-rich spacers is also a short-range interaction and decays with a decay length of the same order of magnitude as the tunneling (2-3 Å, see Fig. 3 and Ref. [1]).

Second Rowell criterion: A representative *I-V* curve taken at RT and the corresponding *dI/dV-V* curve are presented in Fig. 5. They show the typical tunneling-type behavior. The *dI/dV-V* curve is parabolic with its minimum away from $V=0$. These features are characteristic for tunnel junctions with asymmetric barriers and indicate different conditions at the diffused Fe/Si and Si/Fe interfaces, probably due to different interfacial densities of states and/or transmission probabilities of the carriers. There is no evidence for a conductivity anomaly near $V=0$, as previously reported for ferromagnetic junctions with Al-oxide spacers and related to inelastic scattering assisted by magnons and impurities [16].

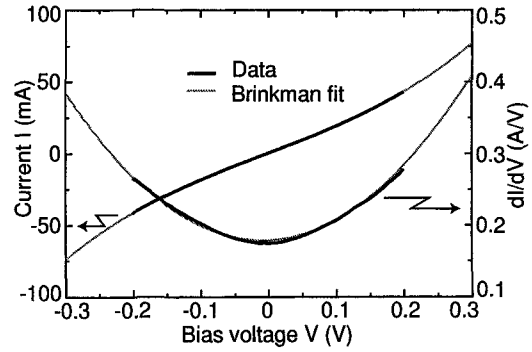

Fig. 5. Measured (black) and fitted (grey) *I-V* and *dI/dV-V* curves of a Fe/Si/Fe junction with $A=100$ μm^2 and $t=15.4$ Å (from [9]).

Similar *I-V* curves can occur when transport is due to another conductivity channel, namely submicron-sized pin-holes, which can mimic elastic tunneling [7]. As we will show below based on an analysis of the temperature dependence of the resistance, this metallic-type channel gives here no significant contribution.

We observe tunneling-type *I-V* curves only for $t>15$ Å, where the voltage drop is sufficient to reveal the non-linear part of *I-V* characteristics. The barrier heights ø derived from Brinkman fits [17] vary from 0.3 to 0.8 eV for different junctions, which all show a definite barrier asymmetry Δø in the range from 0.1 to 0.3 eV. Explicit Brinkman fit results for a series of different junctions and a detailed discussion can be found in Ref. [9]. The variation of the barrier heights could be related to locally different Si contents in the Si-rich spacer. Actually, as it was shown previously [18], an increase of the nominal Si content in a spacer layer to more than 70% leads to an increase of the mean barrier height ø from 0.15 to 0.7 eV. The observed barrier asymmetries Δø are most likely caused by different rates of diffusion at Fe/Si and Si/Fe interfaces [1,4,19].

Third Rowell criterion: A typical temperature

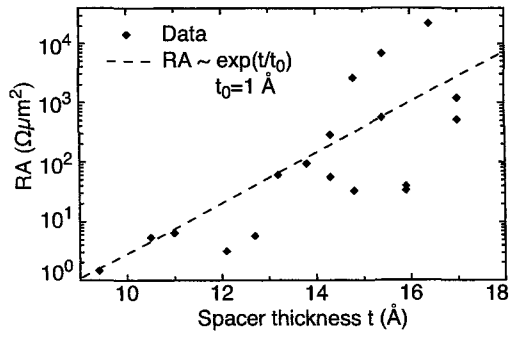

Fig. 4. Dependence of the resistance times area product *RA* on the nominal spacer thickness *t* obtained from Fe(50 Å)/Si(t)/Fe(50 Å) structures. The dashed line corresponds to a characteristic length $t_0=1$ Å (after [9]).

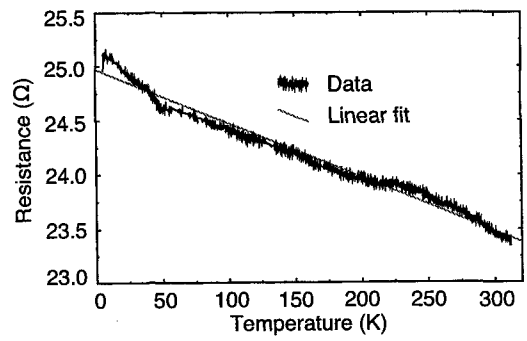

Fig. 6. Dependence of the resistance on temperature for a Fe/Si/Fe junction with $A=22$ μm^2 and $t=17.0$ Å. The solid line is a linear fit that yields a temperature coefficient of -5×10^{-3} ΩK^{-1} (from [9]).

dependence of the zero-bias resistance is presented in Fig. 6. The resistance slightly decreases with temperature and, thus, shows tunneling-type behavior. The total change of resistance from 4 K to RT does not exceed 5-7%. We relate the change of resistance to prevailing direct elastic tunneling, which yields only weak temperature dependence due to the broadening of Fermi distributions. The elastic but resonant tunneling channel is much weaker than the direct one and obeys a decay length, which is twice as large as the decay length of direct tunneling. However, resonant elastic tunneling cannot definitely be excluded for our junctions with t lying in the narrow interval between 14 and 17 Å. Different weights of the contributions from elastic direct and elastic resonant tunneling could lead to the scattering of the *RA* values in Fig. 4. Next, we consider inelastic tunneling based on thermo-activated hopping across impurity states in the barrier. For this channel a strong decrease of resistance with temperature is expected [15]. Thus, this channel is not dominant in our junctions.

With the negative temperature coefficient of the resistance observed in Fig. 6, all three Rowell criteria for direct tunneling are fulfilled, and we can exclude a significant metallic contribution through pin-holes to the electron transport.

3.3 AFC of Fe/BL/Ge-wedge/BL/Fe

First, we prepared Fe/Ge-wedge/Fe trilayers without BL or with only one BL at the bottom or top interface. In all these cases the MOKE hysteresis curves reveal 100% remanent magnetization characteristic for zero or FM coupling. Most likely, strong diffusion at interfaces leads to the formation of magnetic Fe-Ge compounds in the spacer, which cannot mediate AFC [11].

In order to prevent Fe-Ge interdiffusion we deposit Si BL at both interfaces. Typical LEED patterns for all five layers are shown in Fig. 1. The bottom Si BL grows at RT with a similar in-plane lattice constant as Fe(001).

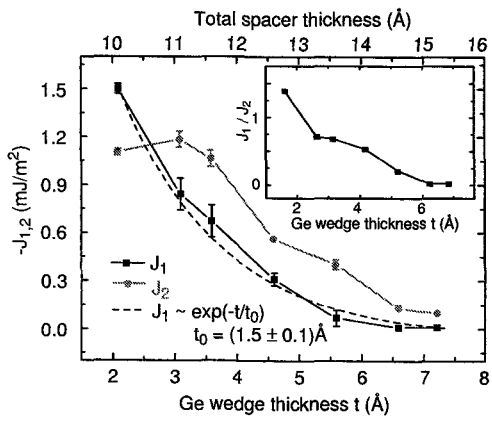

Fig. 7. Bilinear (J_1, black) and biquadratic (J_2, grey) coupling constants *versus* nominal Ge thickness t for a wedge-type Fe(50 Å)/Si/Ge(t)/Si/Fe(30 Å) structure with two 4 Å-thick Si BL. The dashed line is an exponential fit and yields a decay length of about 1.5 Å. The upper abscissa gives the total spacer thickness including the Si BL. The inset shows the ratio J_1/J_2 *versus* t (from [10]).

The nominally pure Ge spacers start to grow epitaxially on Si with an in-plane cubic structure and a lattice parameter of about 2.9 Å (a_{Fe}=2.87 Å). For Ge thicknesses t<6 Å we observe LEED patterns for the Ge spacer, the top BL, and the top Fe layer. Thus, we obtain epitaxial growth of the whole structure.

Figure 7 shows the dependence of the interlayer exchange coupling constants J_1 and J_2 on the thickness of the Ge spacer t for a sample with two BL. The bilinear coupling constant $|J_1|$ quickly drops with t and can be described by an exponential decay with a decay length of about t_0=1.5 Å (dashed line in Fig. 7). The biquadratic term $|J_2|$ is smaller than $|J_1|$ only for t<3 Å. However, the biquadratic coupling is dominating for all Ge thicknesses because $|J_1|<2|J_2|$ (see inset of Fig. 7), and the layer magnetizations are canted in the remanent state, even for smallest t. The likely reason for the observed strong biquadratic coupling is the competition between bilinear coupling and FM coupling due to magnetic bridges [20,21]. The onset of SK hillock growth at Ge thicknesses t>6 Å reduces the efficiency of the FM bridge annihilation upon further Ge deposition. In this context, it is interesting to note that the vanishing of J_1 and the prevalence of J_2 around t=6 Å coincide with the disappearance of the LEED spots.

3.4 AFC of Fe/Si-Ge-multilayer/Fe

In a next step, we prepare samples of the form Fe/Si/Ge.../Fe with N alternating Si and Ge sublayers (Si-Ge-multilayer) as spacers. We observe LEED patterns similar in quality to Fig. 1, even for larger spacer thicknesses than for the Ge-wedge. Figure 8 depicts as an example the MOKE hysteresis loop of a sample with N=6. The grey line is a fit yielding J_1 and J_2 as indicated. J_1 is dominating ($|J_1|>2|J_2|$), and thus the hysteresis loop exhibits a plateau for $|H|$<30 mT due to perfect antiparallel alignment (arrows in Fig. 8). The step at H=0 arises from the different Fe thicknesses. Such a plateau is not observed for the samples with Ge embedded between BL, where biquadratic coupling dominates (inset of Fig. 8). In Fig. 9 we present the dependence of the coupling constants derived from fitting MOKE loops on the number N of sublayers. The

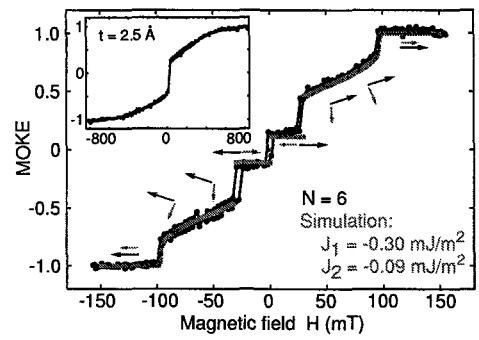

Fig. 8. Experimental (black) and fitted (grey) MOKE hysteresis loop of a sample with an N=6 Si-Ge-multilayer spacer: Fe(50 Å)/Si/Ge/Si/Ge/Si/Ge/Fe(30 Å). All Si and Ge layers are 2 Å thick. Arrows indicate the magnetization alignment obtained from the fitting. Inset: Hysteresis loop of a wedge-type Fe(50 Å)/Si/Ge(t)/Si/Fe(30 Å) sample at t=2.5 Å (from [10]).

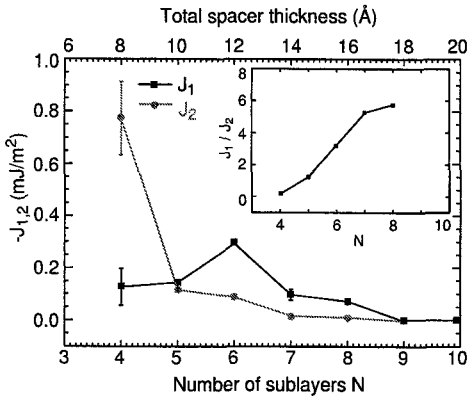

Fig. 9. Bilinear (J_1, black) and biquadratic (J_2, grey) coupling constants *versus* the number N of 2 Å-thick Si and Ge sublayers in the multilayer spacer for structures of the form Fe(50 Å)/Si/Ge.../Fe(30 Å). The upper abscissa gives the total spacer thickness in Å. The inset shows the ratio J_1/J_2 *versus* t (from [10]).

interlayer coupling is FM for smallest spacer thicknesses (N<4) and becomes due to FM bridges prevailing 90°-coupling for N=4, where $J_2 \approx 6J_1$. For N=5, J_1 and J_2 are comparable. The increase of $|J_1|$ from N=4 to 6 and the simultaneous steep decrease of J_2 is due to the transition from FM coupling first to competing FM and antiferromagnetic interactions giving rise to 90°-coupling [20,21] and further to dominant AFC for N=6 to 8. Finally, for N=9 AFC is negligible, and both FM layers are aligned parallel to the field H.

The maximum of $|J_1|$ of about 0.3 mJ/m^2 is reached for N=6 corresponding to a total spacer thickness of 12 Å. Taking for the Ge-wedge samples the thickness of the BL into account, a total spacer thickness of 12 Å corresponds to t=4 Å. Thus, the strength of the bilinear coupling across Si-Ge-multilayer is roughly comparable to that across embedded Ge-wedges of similar total thickness (Fig. 7). The bilinear coupling extends to about the same total spacer thicknesses: 16 Å (N=8) for the multilayer spacers and 15 Å (t=7 Å) for the embedded Ge-wedges (Fig. 7). However, the evolution of J_2 is completely different for the two types of samples: for multilayer spacers it is very strong for small N due to strong intermixing, but drops rapidly and becomes secondary for larger N. This different behavior is best recognized by comparing the dependence of the J_1/J_2 ratios in the insets of Figs. 7 and 9. We relate these observations to the well-established mechanism of strain stabilization in Si/Ge multilayers [22] that shifts the transition to the SK hillock growth to larger thicknesses, as indicated by our LEED data. Thus, the Si-Ge-multilayer spacers show improved growth compared to the Ge-wedge samples, once they are thick enough (N>5) to sufficiently suppress the formation of FM bridges.

4. DISCUSSION

Epitaxial, AF coupled Fe/Si/Fe junctions fulfill the necessary and sufficient Rowell criteria for direct elastic electron tunneling: The junctions show (i) a strong increase of area times resistance product with spacer thickness, (ii) parabolic conductivity *versus* voltage dependencies, and (iii) small negative temperature coefficients of the resistance. Thus, we could show for AF coupled Fe/Si/Fe junctions, that there is no significant contribution to the conductivity caused by pin-holes. The experimentally proven coexistence of both strong AFC and electron transport *via* direct tunneling across nominally pure Si spacers is an important piece of information for a better understanding of the mechanism of strong AFC across Si spacers.

Furthermore, we have shown that epitaxial Fe/spacer/Fe structures containing Ge in the spacer demonstrate AFC by studying nominally pure Ge-wedges embedded between two Si BL as well as Si-Ge-multilayer spacers. The coupling strengths are of the order of 1 mJ/m^2 and decay on a length scale of less than 2 Å. Biquadratic coupling is observed for both sample types at small spacer thicknesses. However, the biquadratic contribution vanishes much faster for the multilayer spacers as evidenced by the different behavior of the J_1/J_2 ratios. We believe that this is due to strain stabilization in the layered Si-Ge structure [22]. The resulting better growth quality for sufficiently large N with suppressed impact of FM bridges gives rise to almost pure bilinear coupling with a perfect antiparallel alignment.

The direct comparison of AFC across Si and Ge-containing spacers is impaired by the need for Si BL or layering of Si and Ge for the Ge-containing spacers. Nevertheless, we found that the decay lengths of J_1 are very similar and of the order of interatomic distances. The coupling strengths across epitaxial Si and Ge clearly exceed the corresponding values for amorphous spacers by 3 orders of magnitude [23,24]. In the case of nominally pure Si spacers, the coupling also exceeds the values previously found for various Fe/$Fe_{1-x}Si_x$/Fe structures [1,3,18,25,26]. We are not aware of any published AFC strengths across crystalline Ge to compare with. Our data show, that the coupling across Ge-containing interlayers is weaker than across Si, *e.g.* at 12 Å total spacer thickness 3 or 5 times weaker for Ge-wedges and Si-Ge-multilayers, respectively. These reduced coupling strengths are not surprising in view of the additional interfaces between Ge and Si boundary layers or Si sublayers and are probably dominated by the number of interfaces rather than by intrinsic differences between Si and Ge. The observed similarities for Si- and Ge-wedges and the fact that Si-Ge-multilayer spacers also behave similarly indicate a common, intrinsic origin for the antiferromagnetic bilinear coupling. The different behaviors of the biquadratic coupling —J_1/J_2 increasing with t for Si [1] and Si-Ge-multilayers (inset of Fig. 9), but decreasing for Ge-wedges (inset of Fig. 7)— are due to extrinsic influences, *e.g.* pin-holes and growth quality as discussed in Sects. 3.3. and 3.4.

5. CONCLUSIONS

The presented results indicate that relatively strong AFC is a common feature of well-ordered, epitaxial spacer layers consisting of semiconducting elements. A quantitative theoretical description of strong AFC across semiconductor spacers —representing the intermediate case between metallic and insulating spacers— is highly desired.

REFERENCES

[1] R.R. Gareev, D.E. Bürgler, M. Buchmeier, R. Schreiber and P. Grünberg, J. Magn. Magn. Mater. **240**, 235-237 (2002).
[2] J. Faure-Vincent, C. Tiusan, C. Bellouard, E. Popova, M. Hehn, F. Montaigne, and A. Schuhl, Phys. Rev. Lett. **89**, 107206 (2002).
[3] R.R. Gareev, D.E. Bürgler, M. Buchmeier, D. Olligs, R. Schreiber, and P. Grünberg, Phys. Rev. Lett. **87**, 157202 (2001).
[4] R.R. Gareev, D.E. Bürgler, M. Buchmeier, R. Schreiber, and P. Grünberg, Appl. Phys. Lett. **81**, 1264-1266 (2002).
[5] R.R. Gareev, D.E. Bürgler, M. Buchmeier, R. Schreiber, and P. Grünberg, Trans. Magn. Soc. Jpn., **2**, 205-206 (2002).
[6] P. Bruno, Phys. Rev. B **52**, 411-439 (1995).
[7] D.A. Rabson, B.J. Jönsson-Åkerman, A.H. Romero, R. Escudero, C. Leighton, S. Kim, and I.K. Schuller, J. Appl. Phys. **89**, 2786-2790 (2001).
[8] J.J. Åkerman, R. Escudero, C. Leighton, S. Kim, D.A. Rabson, R.W. Dave, J.M. Slaughter, and I.K. Schuller, J. Magn. Magn. Mater. **240**, 86-91 (2002).
[9] R.R. Gareev, L.L. Pohlmann, S. Stein, D.E. Bürgler, and P.A. Grünberg, J. Appl. Phys. **93**, 8038-8040 (2003).
[10] R.R. Gareev, D.E. Bürgler, R. Schreiber, H. Braak, M. Buchmeier, and P.A. Grünberg, Appl. Phys. Lett. **83**, 1806-1808 (2003).
[11] J.J. de Vries, J. Kohlhepp, F.J.A. den Broeder, P.A. Verhaegh, R. Jungblut, A. Reinders, and W.J.M. de Jonge, J. Magn. Magn. Mater. **165**, 435-438 (1997).
[12] Y.-W. Mo, D.E. Savage, B.S. Swartzentruber, and M.G. Lagally, Phys. Rev. Lett. **65**, 1020-1023 (1990).
[13] M. Buchmeier, B.K. Kuanr, R.R. Gareev, D.E. Bürgler, and P. Grünberg, Phys. Rev. B **67**, 184404 (2003).
[14] R.J.M. van de Veerdonk, J. Novak, R. Meservey, J.S. Moodera, and W.J.M. de Jonge, Appl. Phys. Lett. **71**, 2839-2841 (1997).
[15] Y. Xu, D. Ephron, and M.R. Beasley, Phys. Rev. B **52**, 2843-2859 (1995).
[16] J. S. Moodera and G. Mathon, J. Magn. Magn. Mater. **200**, 248-273 (1999).
[17] W.F. Brinkman, R.C. Dynes, and J.M. Rowell, J. Appl. Phys. **41**, 1915-1921 (1970).
[18] Y. Endo, O. Kitakami, and Y. Shimada, J. Appl. Phys. **87**, 6836-6838 (2000).
[19] R. Kläsges, C. Carbone, W. Eberhardt, C. Pampuch, O. Rader, T. Kachel, and W. Gudat, Phys. Rev. B **56**, 10801-10804 (1997).
[20] J.C. Slonczewski, J. Appl. Phys. **75**, 6474 (1994).
[21] J.F. Bobo, H. Kikuchi, O. Redon, E. Snoeck, M. Piecuch, and R.L. White, Phys. Rev B **60**, 4131-4141 (1999).
[22] S.C. Jain and W. Hayes, Semicond. Sci. Technol. **6**, 547-576 (1991).
[23] B. Briner and M. Landolt, Phys. Rev. Lett. **73**, 340-343 (1994).
[24] P. Walser, M. Schleberger, P. Fuchs, and M. Landolt, Phys. Rev. Lett. **80**, 2217-2220 (1998).
[25] E.E. Fullerton, J.E. Mattson, S.R. Lee, C.H. Sowers, Y.Y. Huang, G. Felcher, S.D. Bader, and F.T. Parker, J. Magn. Magn. Mater. **117**, L301-L306 (1992).
[26] J.J. de Vries, J. Kohlhepp, F.J.A. den Broeder, R. Coehoorn, R. Jungblut, A. Reinders, W.J.M. de Jonge, Phys. Rev. Lett. **78**, 3023-3026 (1997).

(Received October 8, 2003; Accepted February 3, 2004)